The phase diagram and optical properties of $La_{1-x}Sr_xMnO_3$ for $x \leqslant 0.2$

M. Paraskevopoulos[a], F. Mayr[a], C. Hartinger[a], A. Pimenov[a], J. Hemberger[a], P. Lunkenheimer[a], A. Loidl[a,*], A.A. Mukhin[b], V.Yu. Ivanov[b], A.M. Balbashov[c]

[a]*Experimentalphysik V, Elektronische Korrelationen und Magnetismus, Institut für Physik, Universität Augsburg, D-86159 Augsburg, Germany*
[b]*General Physics Institute of the Russian Acad. Sci. 117942 Moscow, Russia*
[c]*Moscow Power Engineering Institute, 105835 Moscow, Russia*

Abstract

We report on detailed susceptibility, magnetization and magnetoresistance studies in $La_{1-x}Sr_xMnO_3$ for $x \leqslant 0.2$. We arrive at a phase diagram which shows a ferromagnetic and insulating ground state for $0.1 \leqslant x \leqslant 0.15$, followed by a canted antiferromagnetic phase at higher temperatures. The ferromagnetic transition is strongly coupled to a structural transition from a Jahn–Teller distorted phase to a pseudocubic orthorhombic phase, and is accompanied by the appearance of large positive magnetoresistance effects. We interpret the rich phase diagram close to $x = \frac{1}{8}$ in terms of orbital ordering, due to an interplay of superexchange interactions and Jahn–Teller distortions. In addition, we report on the temperature dependence of phonon spectra and on optical conductivities. The temperature dependence of bending and stretching modes clearly indicate the structural and magnetic-phase transitions. The optical conductivities are explained in terms of small polaron absorption.

Keywords: Perovskite manganites; Magnetic properties; Optical properties; Magnetoresistance

1. Introduction

It is now half a century ago that Jonker and van Santen [1] demonstrated that the manganite perovskites $(La^{3+}Mn^{3+}O_3^{2-})_{1-x}(A^{2+}Mn^{4+}O_3^{2-})_x$ reveal an interesting and puzzling phase diagram [1,2]. It was de Gennes [3] to establish the close connection of electrical and magnetic properties via an interplay of Mn–O–Mn superexchange (SE) interactions with Zener's double-exchange (DE) [4]. Driven by an increasing concentration of mobile holes, the insulating (I) and antiferromagnetic (AFM) structure passes via a canted AFM (CA) structure to a purely metallic (M) and ferromagnetic (FM) ground state [3]. Recently, an overwhelming interest in the manganites arose due to the observation of negative colossal magnetoresistance (CMR) close to $x \simeq 0.3$ [5–7]. These CMR effects at the FM phase transition were explained within extended double exchange models [8], which took Jahn–Teller (JT) distortions into account indicating the importance of structural aspects [9].

* Corresponding author. Tel.: + 49-821-598-3600; fax: + 49-821-598-3649.
E-mail address: alois.loidl@physik.uni-augsburg.de (A. Loidl)

An early structural phase diagram has been presented by Bogush et al. [10]. On decreasing temperature pure $LaMnO_3$ reveals the sequence rhombohedral (R), orthorhombic (O) and finally another orthorhombic structure (O′). In the O phase the three octahedral Mn–O bond lengths are almost equal, while in the JT-distorted O′ phase, these bond lengths become anisotropic. An electronic phase diagram for $La_{1-x}Sr_xMnO_3$ ($x \leqslant 0.5$) has been published by Urushibara et al. [11]. That the (x, T) phase diagram in $La_{1-x}Sr_xMnO_3$ for low doping concentrations ($x < 0.2$) is even more complex, has been established by Kawano et al. [12,13], Yamada et al. [14] and Zhou et al. [15]. Guided by the classical conjectures of competing DE and SE interactions [3], in these phase diagrams it has been explicitly assumed that the regime where the resistivity decreases with decreasing temperature ($d\rho/dT > 0$) is metallic and reveals a simple FM spin arrangement and that the low-temperature I ground state ($d\rho/dT < 0$) exhibits a CA structure for $x \leqslant 0.15$. Based on systematic magnetic susceptibility, magnetization and magnetoresistance (MR) experiments on single-crystalline $La_{1-x}Sr_xMnO_3$ we provide experimental evidence that all these phase diagrams are not correct for $x \leqslant 0.2$. Our results reveal that in this doping regime orbital order and SE interactions play a more fundamental role than the ferromagnetic DE interactions.

In addition, we present the temperature dependence of characteristic infrared (IR) active phonon modes. The phonon eigenfrequencies as well as the phonon damping show significant anomalies at the structural and magnetic transitions. Furtheron microwave and optical-conductivity experiments were conducted revealing the complete frequency range from DC up to 200 THz (≈ 1 eV $\approx 8000\ cm^{-1}$). For $x \leqslant 0.15$ no indication of a Drude peak is observed and variable-range-hopping (VRH) conductivity below the phonon bands and polaron absorption above the phonon frequencies dominate the optical spectra.

2. Experimental details

Well characterized single crystals of $La_{1-x}Sr_xMnO_3$ with concentrations $0 \leqslant x \leqslant 0.2$, were grown by the floating zone method as described in Ref. [16]. To establish a detailed and complete phase diagram, the magnetic susceptibility and magnetization was measured using an Oxford AC-susceptometer in fields up to 140 kOe and for temperatures 1.5 K $< T <$ 300 K and a quantum design DC SQUID magnetometer (50 kOe, 1.5 K $< T <$ 800 K). The magnetoresistance has been measured with a standard four-probe technique in an Oxford cryostat and in fields up to 140 kOe.

The complex conductivity has been recorded using a HP 4291 impedance analyzer for frequencies 1 MHz $\leqslant \nu \leqslant$ 1.8 GHz. The microwave conductivity has been measured at 7.3 GHz utilizing a microwave perturbation technique within an ^{4}He-flow cryostat. Transmission experiments in the frequency range from 100 GHz ($\approx 3\ cm^{-1}$) to 1 THz ($\approx 30\ cm^{-1}$) were performed utilizing a set of backward-wave-oscillators. These measurements were performed in a Mach–Zehnder configuration, which allows measurements of transmission and phase shift.

In the IR regime the temperature-dependent conductivity was determined via reflectivity measurements using a Bruker IFS 113v Fourier transform interferometer. The spectral range from 2 meV ($\approx 25\ cm^{-1}$) to 1 eV($\approx 8000\ cm^{-1}$) was covered utilizing a suitable set of sources, beamsplitters, windows and detectors. The sample was placed in the exchange gas of a ^{4}He-bath cryostat.

3. Results and discussion

3.1. Magnetic susceptibility, magnetization and magnetoresistance measurements

In Fig. 1, the magnetic AC-susceptibility of $La_{1-x}Sr_xMnO_3$ is plotted vs. temperature for various doping levels. In the low doping regime (inset of Fig. 1), a pronounced peak at about 125–140 K indicates the paramagnetic (PM) to CA transition. For $x < 0.1$ the transition temperature T_{CA} shifts towards lower temperatures as the Sr concentration is increased. For the samples with $x = 0.1$ and 0.125 one can identify two magnetic transitions ($x = 0.1$: $T_{CA} = 150$ K, $T_C = 105$ K; $x = 0.125$: $T_{CA} = 180$ K, $T_C = 140$ K). A structural transition

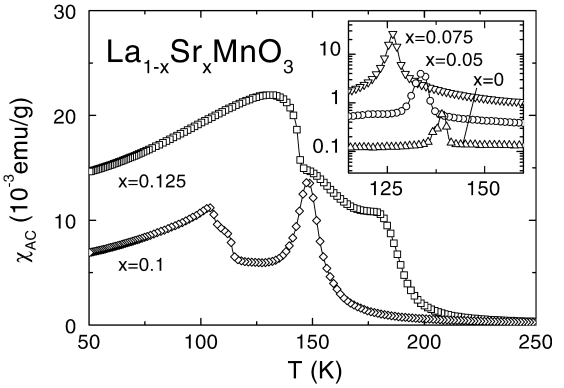

Fig. 1. AC susceptibility vs. temperature in $La_{1-x}Sr_xMnO_3$ for concentrations $x = 0.1, 0.125$. The inset shows the susceptibilities for $x = 0$, 0.05 and 0.075 on a semi-logarithmic scale.

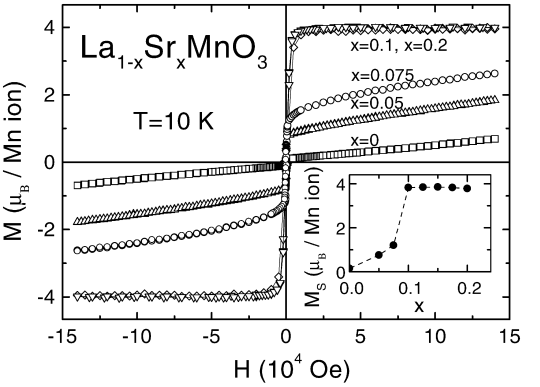

Fig. 2. Magnetization vs. magnetic field for $La_{1-x}Sr_xMnO_3$ for concentrations $x = 0$, 0.05, 0.075, 0.1 and 0.2 at 10 K. The inset shows the spontaneous magnetization M_S as a function of x.

from the JT distorted O′ phase into a pseudocubic O″ phase [17,18] coincides with the low-temperature magnetic transition. These transitions temperatures shift to higher values with increasing Sr concentration. For $x = 0.15$ this sequence of structural and magnetic transitions appears in a narrow temperature range which can hardly be resolved. The structural phase transition at higher temperatures and the FM transitions for $x > 0.15$ were studied in susceptibility and resistivity measurements.

Fig. 2 shows the magnetization at 10 K for various compositions ($x \leqslant 0.2$) as a function of the magnetic field. The samples with $x < 0.1$ are in a CA phase, which can be concluded from the fact that there exists a spontaneous magnetization M_S, followed by a linear increase of the magnetization M as the magnetic field is further raised. There is no sign of saturation even at an applied field of 14 T. This behavior corresponds to the predictions of de Gennes [3] for the manganites in the canted phase. The basic effect is that the external magnetic field enforces a continuous reduction of the canting angle. In addition, the initial value of the spontaneous FM magnetization increases with x, a fact that directly demonstrates the reduction of the canting angle on hole doping. We clearly have to state that on the basis of our measurements we cannot decide wether we have a canted or mixed phase (i.e. phase separation). However, recently Kumagai et al. [19] based on ^{139}La-NMR data have shown that the magnetic structure of lightly doped $La_{1-x}Sr_xMnO_3$ is microscopically homogeneous. For doping rates $x \geqslant 0.1$ we find the typical characteristics of a FM state with the magnetization reaching saturation within 20 kOe. The complete parallel alignment of the Mn^{3+}/Mn^{4+} spins is indicated by the values of M_S which approach the classical spin-only value (inset of Fig. 2).

In the following we concentrate on the sample $La_{0.9}Sr_{0.1}MnO_3$, although the same conclusions can also be drawn for $x = 0.125$. In order to understand the evolution of the different magnetic and electronic states as a function of temperature and magnetic field, we have measured the magnetization and the magnetoresistance up to 140 kOe at various temperatures. Fig. 3a shows some representative magnetization results. For $T > T_{CA} = 150$ K the magnetization curves reveal the signature of a typical PM. Below T_{CA} we observe a linear increase of the magnetization on increasing field, characteristic for a CA. However, at a given critical field the mangetization jumps to higher values. A closer inspection reveals two subsequent transitions probably resulting from the twinning of our crystal. At these jumps the sample undergoes a magnetic transition into a FM state reaching full magnetization. With decreasing temperature this anomalies are shifted to lower fields and finally disappear below $T_C = 105$ K. For $x = 0.1$ the field

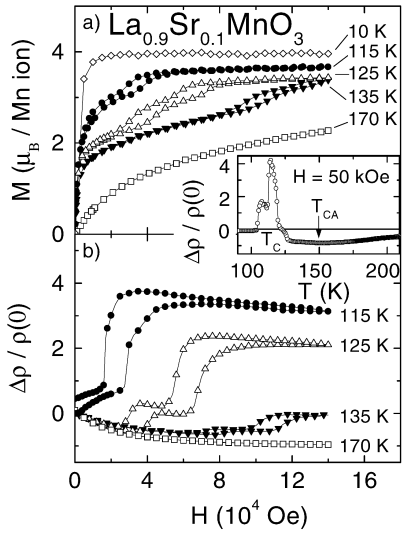

Fig. 3. (a) Magnetization vs. field as observed in $La_{0.9}Sr_{0.1}MnO_3$ at different temperatures. (b) Isothermal MR for $x = 0.1$ as function of external field. The inset shows the T-dependence of the MR at 50 kOe.

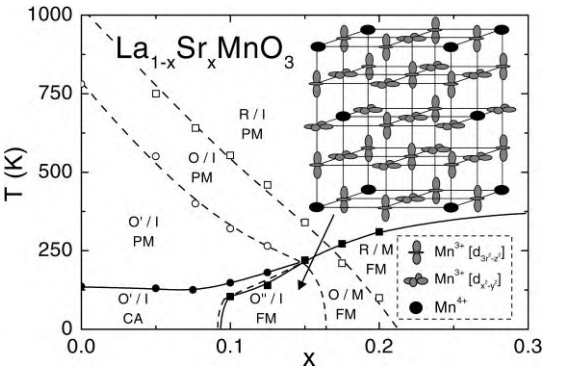

Fig. 4. (x, T) phase diagram of $La_{1-x}Sr_xMnO_3$. The structural (O, O′, O″, R), magnetic (PM, CA, FM) and electronic (M, I) phases are indicated. Open symbols (dashed lines) denote structural phase boundaries, solid symbols (full lines) denote magnetic phase boundaries. The inset shows the orbital ordering which yields a FM ground state and is in accord with the polaron ordered state proposed by Yamada et al. [11].

dependence of the magnetoresistance (MR: $\Delta\rho/\rho(0) = [\rho(H) - \rho(0)]/\rho(0)$) is shown in Fig. 3b for various temperatures. For temperatures $T > T_C$ we find negative MR effects. Small negative MR effects again appear for $T < T_C$. In the vicinity of T_C large positive MR effects appear, indicating that the FM ground state is more insulating than the CA phase. Again two subsequent jumps as a function of increasing field can be seen. Both jumps induce higher resistivity states and correspond to those observed in the magnetization curves (see Fig. 3a). For $x = 0.125$ these jumps are weaker and for $x = 0.15$ only negative CMR effects have been observed in agreement with previous published results [9]. To further investigate these large positive MR effects, the temperature dependence of the magnetoresistance measured in an external field $H = 50$ kOe is plotted in the inset of Fig. 3. An increase in resistivity at T_C by a factor of four is clearly visible. Around T_{CA} the typical negative MR effect can be seen. The positive MR is largest for $x = 0.1$, significantly smaller for $x = 0.125$ and finally disappears for $x \geqslant 0.15$. In summary, the magnetoresistance measurements indicate a large positive MR at the transition O′/CA → O″/FM, while negative MR effects appear close to the O′/PM → O′/CA and O/PM → O/FM phase boundaries.

Based upon these experimental results we constructed a structural, magnetic and electronic phase diagram (Fig. 4). At low temperatures and low concentrations ($x < 0.1$) we find an insulating orthorhombic phase O′ which reveals canted antiferromagnetism. The phase diagram becomes much more complicated at higher Sr concentrations. Our results provide clear experimental evidence that for $0.1 \leqslant x \leqslant 0.15$ the ground state is a FM insulator and for $x = 0.1$ and 0.125 is followed by a canted spin state at elevated temperatures. Using neutron diffraction techniques, Argyriou et al. [20] have monitored the temperature dependence of the canting angle Θ for $x = 0.125$ and observed a continuous decrease below T_{CA} and a lock-in like phenomenon of the canting angle at approximately 20° below 160 K. At the O′O″ phase boundary which is coupled with the CA → FM transition, the resistivity steeply increases. For $x > 0.17$ the ground state is a FM metal revealing an O structure for $x < 0.2$ and a R structure for $x > 0.2$.

We summarize the most important experimental results of this section. It is obvious that the

transition from the CA and JT distorted O′ phase to the pseudocubic O″ phase, which is intimately coupled to a transition into an insulating FM ground state, calls for a different picture as it can be given by the interplay of JT distortions and DE interactions alone.

For undoped $LaMnO_3$ the magnetic properties can be understood taking only the predominant JT-distortion of the MnO_6 octahedra into account. The double degeneracy of the e_g orbitals is lifted by a long-range cooperative Jahn–Teller distortion resulting in an ordering of the $d_{3r^2-z^2}$ orbitals as argued by Solovyev et al. [21] and has recently been confirmed experimentally by Murakami et al. [22]. As a consequence of this JT driven orbital ordering the A-type AFM state is established below T_N. The possibility of orbital ordering in transition-metal oxides due to exchange interactions different than that resulting from JT distortions [23,24] was first pointed out by Roth [25,26] and has been extensively studied by Kugel and Khomskii [27,28]. It has been shown that in the case of orbital degeneracy two transitions take place, one into an orbitally ordered state and a second into a spin-ordered state, both driven by SE-mechanisms. This SE differs from the ordinary one due to the fact that each electron has four degrees of freedom, two orbital states ($d_{3r^2-z^2}$, $d_{x^2-y^2}$) and two spin states (*spin-up, spin-down*). The presence of intra-atomic exchange (Hund's rule coupling) produces ferromagnetism below the orbital-ordering phase transition [29]. We remark that in the O′ phase the degeneracy of the Mn^{3+} e_g orbitals is lifted by the JT distortion yielding anisotropic SE interactions, which are FM in-plane and AFM out-of-plane [21]. On the other hand, in the pseudocubic O″ phase where the degeneracy is restored, the SE interactions become FM and isotropic.

The phase diagram for $x < 0.1$ can be explained assuming a JT derived O′ phase with strongly anisotropic Mn–O bonds. Dominating anisotropic SE and weak DE interactions establish a canted phase which is directly derived from the A-type AFM of the pure compound. The decrease of $T_{CA}(x)$ in this regime results from a continuous suppression of the JT distortions with increasing hole doping and a concomitant weakening of the anisotropic SE. On the other hand, the increase of $T_{CA}(x)$ upon doping for $0.1 \leqslant x \leqslant 0.15$ signals that the magnetic state is now driven by 3D ferromagnetic DE interactions which are perturbed by weak antiferromagnetic SE interactions, yielding a CA state. An increase of the hopping matrix elements due to enhanced DE interactions is evidenced by the decrease in resistivity at T_{CA}, which is not present for the $x < 0.1$ samples [11]. However, the DE mechanism is not strong enough to create a metallic phase. It has been demonstrated recently that for $0.1 \leqslant x \leqslant 0.15$ the regime with $d\rho/dT > 0$ still is insulating and characterized by hopping of localized charge carriers [30].

3.2. Optical investigations and microwave conductivities

3.2.1. Phonon spectra

Most of the optical investigations focused on the optical conductivities in the FIR regime paying only little attention to the temperature dependence of the phonon spectra. The cubic ABO_3 perovskites usually display three main IR bands located at approximately 180, 350 and 550 cm^{-1}. The lowest mode represents an external vibration of the A ions against the BO_6 octahedra. The bending mode at 350 cm^{-1} comes from an internal motion of the B and O ions in a particular direction against the oxygen ions located within a plane perpendicular to this direction. This mode is strongly affected by changes of the B–O–B bond angles. Finally, the high-frequency stretching mode corresponds to a vibration of the B ions against the oxygen octahedra and is sensitive to the B–O bond lengths.

The Raman and infrared phonons of ceramic $LaMnO_3$ were studied by Abrashev et al. [31] at room temperature and were compared to the isostructural compound $LaAlO_3$. Three characteristic bands located at 152, 315 and 586 cm^{-1} were detected. The temperature dependencies of the internal phonon modes of $La_{0.7}Ca_{0.3}MnO_3$ were presented by Kim et al. [32]. At room temperature the three IR active modes were detected close to 165, 330 and 575 cm^{-1}. With decreasing temperature the two high-frequency modes increased significantly below T_C, while the low-frequency external mode remained unshifted.

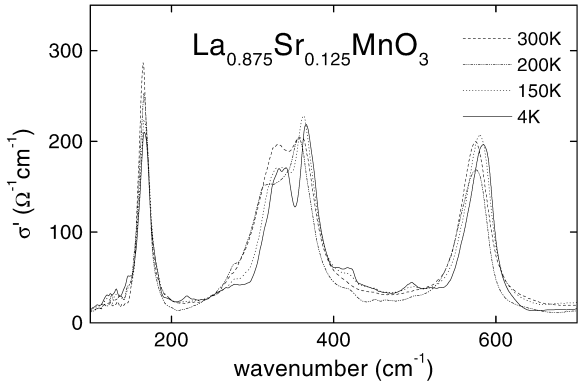

Fig. 5. Optic phonon modes of $La_{0.875}Sr_{0.125}MnO_3$ at different temperatures.

Fig. 5 shows the present experimental IR results of the phonon modes in $La_{0.875}Sr_{0.125}MnO_3$. Here we plotted the real part of the conductivity σ' vs. the phonon wave numbers at different temperatures. Clearly, three bands can be identified, at room temperature located roughly at 165, 330 and 575 cm^{-1}. The band at intermediate frequencies is splitted due to the orthorhombic distortions. In addition, side bands evolve at low temperatures which possibly indicate a further structural transition with a doubling of the Brillouin zone. Fig. 5 also provides experimental evidence that all phonon modes show shifts in frequency, in damping and in intensity. The conductivity spectra were modeled using four Lorentz oscillators, in an attempt to describe the IR band at intermediate frequencies by two phonon contributions (v_2, v_3), although a third mode may be involved. In Fig. 6 we show the temperature dependencies of the phonon frequencies and of the damping constants for the external mode (v_1, γ_1), the bending (v_3, γ_3) and the stretching mode (v_4, γ_4). At the same time we indicate the phase boundaries. It is obvious that the bending and stretching modes reveal an increase by almost 3% at the phase boundary from the PM to the CA transition while the external mode only increases smoothly by only 1.5 in the complete temperature range. At present it is unclear if the decrease of the bending and stretching frequencies at the phase boundary from the O to the O′ phase is significant. However, there is a strong increase of the eigenfrequencies of both

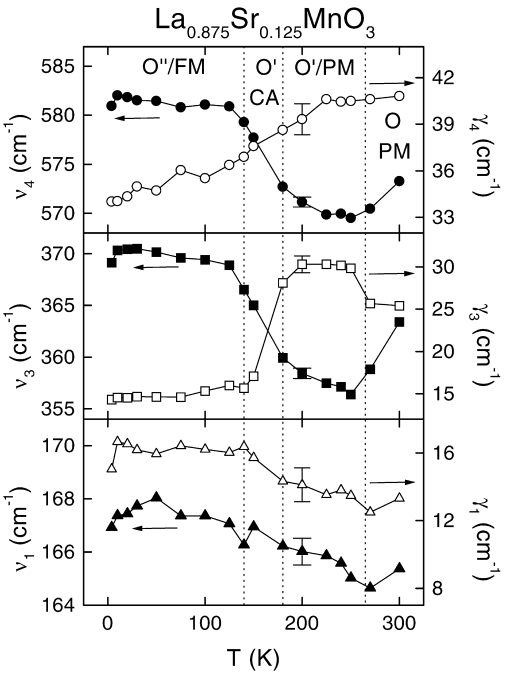

Fig. 6. Temperature dependence of the phonon eigenfrequencies v_i (left scale) and damping constants γ_i (right scale) for $La_{0.875}Sr_{0.125}MnO_3$.

modes at the magnetic phase boundary which saturates in the FM and pseudocubic O″ phase. The damping of the modes behaves rather unusual. The damping of the external mode, v_1, increases steadily. The damping of the bending mode, v_3, increases at the structural phase transition from the orthorhombic O phase to the JT distorted O′ phase and strongly decreases at the magnetic phase boundary from the CA to the FM phase. Finally, the damping constant of the stretching mode, v_4, slightly decreases on passing the magnetic phase transitions. A significant decrease of the phonon-damping constants at the FM phase boundary has been predicted by Lee and Min [33], in their calculations using a polaron model including double-exchange interactions.

3.2.2. *Optical and microwave conductivities*

A vast number of conductivity spectra have been reported on the manganites. In pure $LaMnO_3$, with a long-range Jahn–Teller distortion, the e_g bands splits into two subbands separated by

approximately 1.9 eV [34]. Of course direct d–d transitions are dipole forbidden. However, it is believed that the lower subband hybridizes considerably with the oxygen 2p bands yielding finite dipole transition-matrix elements. Focusing on the $LaMnO_3$ doped with strontium, an early systematic study has been performed by Okimoto et al. [35] on single crystals for strontium concentrations $x = 0, 0.1, 0.175$ and 0.3. For $x = 0.1$ they observed an increase of mid-infrared conductivity close to 0.5 eV which continuously increased on decreasing temperatures. This peak in the conductivity spectrum has been qualitatively explained by Millis et al. [36] as an electronic transition from an occupied site (Mn^{3+}) to an adjacent unoccupied site (Mn^{4+}). A further investigation for polycrystalline samples with $x = 0.125$ has been reported by Jung et al. [37]. These authors again observed an increase of midgap-state conductivity close to 0.4 eV in addition to the broad interband transition at 1.6 eV. The midgap conductivity was explained in terms of a small polaron whose intensity strongly increases in the magnetically ordered state as the ferromagnetic order yields highly enhanced hopping transition matrix elements.

Fig. 7 shows the optical conductivity as observed in $La_{0.875}Sr_{0.125}MnO_3$ in the complete spectral range from DC up to 200 THz. Clearly, below the phonon frequencies the conductivity steadily increases as function of frequency at all temperatures investigated. This is the characteristic property of charge carriers hopping between localized states. No indications of a Drude peak can be detected, even not in the so-called metallic regime with $(d\rho/dT < 0)$. This effect has been studied in detail by Pimenov et al. [30]. Above the phonon modes the intensity strongly increases, which most probably is a sum of polaron absorption and interband transitions. The temperature dependence of the conductivities as measured at different frequencies in the course of this work are shown in Fig. 8. Astonishingly, above 100 K all curves reveal the same characteristics indicating anomalies at the structural and magnetic phase transitions. Only at low temperatures the conductivities at frequencies below the phonon modes exponentially decrease, while the optical conductivity above the phonon frequencies slightly increases.

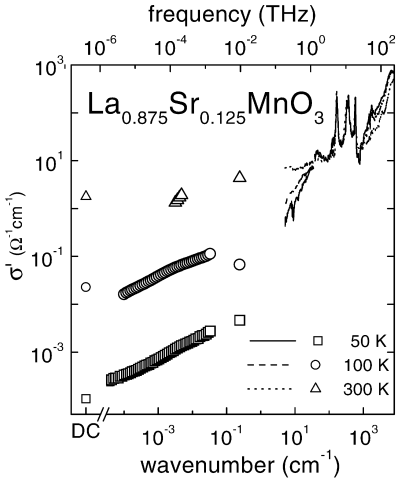

Fig. 7. Frequency dependence of the optical conductivity in $La_{0.875}Sr_{0.125}MnO_3$ at various temperatures.

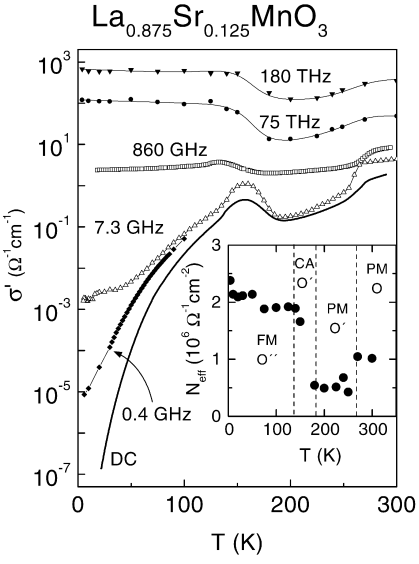

Fig. 8. Temperature dependence of the optical conductivity in $La_{0.875}Sr_{0.125}MnO_3$ at different frequencies from DC to 180 THz. The inset shows the temperature dependence of the optical weight N_{eff} for the conductivity above the phonon eigenmodes.

Here we further report on preliminary results on the optical conductivity in $La_{0.875}Sr_{0.125}MnO_3$ for photon energies below 1 eV. The optical conductivity spectra were obtained by Kramers–Kronig analysis of the reflectivity data. For this

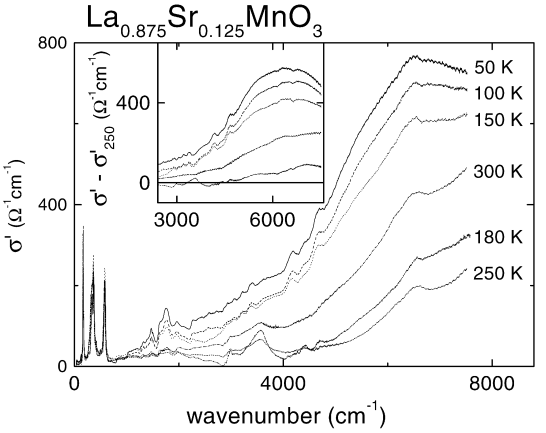

Fig. 9. FIR-optical conductivity in $La_{0.875}Sr_{0.125}MnO_3$ vs. wave number at different temperatures. The inset shows the difference spectra, in which $\sigma(250\ K)$ has been substracted from the conductivities as observed at other temperatures.

analysis we used the data of Okimoto et al. [35] in the range from 1 up to 36 eV. For higher energies a smooth extrapolation to zero was used. The wave number dependence of the real part of the optical conductivity at different temperatures is shown in Fig. 9. Note that at 250 K, where the optical conductivity is lowest, the crystal reveals long-range order Jahn–Teller distortions. At 300 K $La_{0.875}Sr_{0.125}MnO_3$ exhibits the orthorhombic O structure, probably exhibiting a dynamic JT effect, below 180 K magnetic order (canted antiferromagnetism) is established and below 150 K the sample reveals a pseudocubic structure and ferromagnetic order. If we assume that in the Jahn–Teller distorted phase almost pure interband transition are observed, it is reasonable to take this spectrum as background which should be subtracted from the conductivities observed at the other temperatures. This difference spectra are shown in the inset of Fig. 9 and clearly can be interpreted as polaron absorption with a characteristic polaron binding energy of the order of 0.4 eV [38]. Assuming that the position of the peak maximum is directly related to the binding energy, we find that it is considerably shifted to lower energies in the pseudocubic and ferromagnetic O″ phase, as compared to the paramagnetic O phase. Finally, we calculated the optical weight N_{eff}, by summing up the optical conductivity from just above the phonon frequencies up to 8000 wave numbers (i.e. 1 eV). The result is shown as inset in Fig. 8 as function of temperature. Again we find a slight decrease at the OO′ structural phase transition, a strong increase with the onset of magnetic order and only slight changes at the lower structural phase transition. The optical weight also follows the temperature dependence of the DC conductivity, with the significant difference that the polaronic conductivity slightly increases towards low temperatures, while the DC and the microwave conductivities exponentially decrease towards 0 K.

4. Conclusions

It is obvious that the DE mechanism cannot explain the FM and insulating ground state for $0.1 \leqslant x \leqslant 0.15$. We propose that ferromagnetism in this regime is driven by isotropic SE interactions within the insulating pseudocubic phase O″ and it is straightforward to speculate that O″ indicates a new orbitally ordered phase. The structural phase transition which precedes the FM phase indicates a transition from a JT-derived orbital order (O′ phase) to an exchange derived orbital order (O″ phase). The fundamental open question is, how the system overcomes the long-range JT distortions and establish a new orbital order in a pseudocubic phase. The most plausible explanation is that at this point charge order plays an important role [14]. Recently, Ahn and Millis [39] argued that the interplay of charge and orbital order to minimize the lattice energy could be the origin of this ordering. Within this orbital order ferromagnetism is induced via isotropic 3D SE interactions as discussed above. Charge order in the O″ phase also explains the positive MR observed at the O′O″ phase boundary.

At present only speculations about the orbital order in the low-temperature state (O″ phase) can be made, but an alternation of occupied $d_{3r^2-z^2}$ and $d_{x^2-y^2}$ orbitals on neighboring Mn^{3+}-sites appear to be most probable (inset Fig. 4). This antiferro-type orbital ordering would cause a displacement of the O^{2-} ions due to secondary electrostatic interactions [40], yielding alternating long and

short Mn–O bonds. Together with the real space ordering of the Mn^{3+}/Mn^{4+} ions this results in additional superstructure reflections in the diffraction patterns in accordance with the observations of Yamada et al. [14]. Finally for $x \geqslant 0.175$ the DE becomes dominant and a metallic and FM state is established. The orbital liquid picture recently proposed by Ishihara et al. [41] may be appropriate to describe the physics of this phase.

From the phonon spectra we found that the bending and stretching mode reveal significant anomalies in the temperature dependencies and in the damping constants at the phase boundaries. The increase in the eigenfrequencies were considered to result from the change in the electron screening as the temperature decreases below T_C. The observed decrease in the damping constants below the ferromagnetic phase transition has been predicted in a polaron model including double-exchange interactions and electron–phonon couplings [33].

From the frequency dependence of the optical conductivity in an extremely broad frequency range we conclude that for strontium concentrations below $x = 0.15$, at no temperature a Drude peak can be observed. In the temperature range aboved 100 K the conductivities between DC and 200 THz, all resemble the same universal temperature dependence, indicating that the transport in this frequency regime is fully dominated by hopping of localized charge carriers. Finally, the optical conductivities can well be described within a polaron model. The strong increase of all conductivities in the magnetically ordered states obviously result from significantly enhanced hopping matrix elements as a consequence of the ferromagnetic alignment of the spins. The strong decrease at DC, audio and microwave frequencies results from an exponential increase of the thermally induced hopping probability.

Acknowledgements

We acknowledge valuable discussions with K. Samwer. This work has in part be supported by the BMBF under the contract number 13N6917/Elektronische Korrelationen und Magnetismus.

References

[1] G.H. Jonker, J.H. van Santen, Physica 16 (1950) 337.
[2] E.O. Wollan, V.C. Koehler, Phys. Rev. 100 (1955) 545.
[3] P.G. de Gennes, Phys. Rev. 118 (1960) 141.
[4] C. Zener, Phys. Rev. 82 (1951) 403.
[5] K. Chahara, T. Ohno, M. Kasai, Y. Kozono, Appl. Phys. Lett. 63 (1993) 1990.
[6] R. von Helmot, J. Wecker, B. Holzapfel, L. Schulz, K. Samwer, Phys. Rev. Lett. 71 (1993) 2331.
[7] S. Jin, T.H. Tiefel, M. McCormack, R.A. Fastnacht, R. Ramesh, L.H. Chen, Science 264 (1994) 413.
[8] N. Furukawa, J. Phys. Soc. Jpn. 63 (1994) 3214.
[9] A.J. Millis, P.B. Littlewood, B.I. Shraiman, Phys. Rev. Lett. 74 (1995) 5144.
[10] A.K. Bogush, V.I. Pavlov, L.V. Balyko, Cryst. Res. Technol. 18 (1983) 589.
[11] A. Urushibara, Y. Moritomo, T. Arima, A. Asamitsu, G. Kido, Y. Tokura, Phys. Rev. B 51 (1995) 14 103.
[12] H. Kawano, R. Kajimoto, M. Kubota, H. Yoshizawa, Phys. Rev. B 53 (1996) 2202.
[13] H. Kawano, R. Kajimoto, M. Kubota, H. Yoshizawa, Phys. Rev. B 53 (1996) R14 709.
[14] Y. Yamada, O. Hino, S. Nohdo, R. Kanao, Phys. Rev. Lett. 77 (1996) 904.
[15] J.-S. Zhou, J.B. Goodenough, A. Asamitsu, Y. Tokura, Phys. Rev. Lett. 79 (1997) 3234.
[16] A.A. Mukhin, V.Y. Ivanov, V.D. Travkin, S.P. Lebedev, A. Pimenov, A. Loidl, M. Balbashov, JETP Lett. 69 (1998) 356.
[17] L. Pinsard, J. Rodríguez-Carvajal, A.H. Mouden, A. Anane, A. Revcolevschi, C. Dupas, Physica B 234–236 (1997) 856.
[18] L. Pinsard, J. Rodríguez-Carvajal, A. Revcolevschi, J. All. Comp. 262–263 (1997) 152.
[19] K. Kumagai, A. Iwai, Y. Tomioka, H. Kuwuhara, Y. Tokura, A. Yakubovskii, Phys. Rev. B 59 (1999) 97.
[20] D.N. Argyriou, J.F. Mitchell, C.D. Potter, D.G. Hinks, J.D. Jorgensen, S.D. Bader, Phys. Rev. Lett. 76 (1996) 3826.
[21] I. Solovyev, N. Hamada, K. Terakura, Phys. Rev. Lett. 76 (1996) 4825.
[22] Y. Murakami, J.P. Hill, D. Gibbs, M. Blume, I. Koyama, M. Tanaka, H. Kawata, T. Arima, Y. Tokura, K. Hirota, Y. Endoh, Phys. Rev. Lett. 81 (1998) 582.
[23] H.A. Jahn, E. Teller, Proc. R. Soc. A 161 (1937) 220.
[24] H.A. Jahn, Proc. R. Soc. A 164 (1938) 117.
[25] L.M. Roth, Phys. Rev. 149 (1966) 306.
[26] L.M. Roth, J. Appl. Phys. 38 (1967) 1065.
[27] K.I. Kugel, D.I. Khomskii, JETP Lett. 15 (1972) 446.
[28] K.I. Kugel, D.I. Khomskii, JETP 37 (1973) 725.
[29] S. Inagaki, J. Phys. Soc. Jpn. 39 (1975) 596.
[30] A. Pimenov, C. Hartinger, A. Loidl, A.A. Mukhin, V.Y. Ivanov, A.M. Balbashov, Phys. Rev. B 59 (1999) 12 419.
[31] M.V. Abrashev, A.P. Litvinchuk, M.N. Iliev, R.L. Meng, V.N. Popov, V.G. Ivanov, R.A. Chakalov, C. Thomsen, Phys. Rev. B 59 (1999) 4146.
[32] K.H. Kim, J.Y. Gu, H.S. Choi, G.W. Park, T.W. Noh, Phys. Rev. Lett. 77 (1996) 1877.

[33] J.D. Lee, B.I. Min, Phys. Rev. B 55 (1997) 12 454.
[34] J.H. Jung, K.H. Kim, D.J. Eom, T.W. Noh, E.J. Choi, J. Yu, Y.S. Kwon, Y. Chung, Phys. Rev. B 55 (1997) 15489.
[35] Y. Okimoto, T. Katsufuji, T. Ishikawa, T. Arima, Y. Tokura, Phys. Rev. B 55 (1997) 4206.
[36] A.J. Millis, R. Mueller, B.I. Shraiman, Phys. Rev. B 54 (1996) 5405.
[37] J.H. Jung, K.H. Kim, H.J. Lee, J.S. Ahn, N.J. Hur, T.W. Noh, M.S. Kim, J.-G. Park, Phys. Rev. B 59 (1999) 3793.
[38] D. Emin, Phys. Rev. B 48 (1993) 13 691.
[39] K.H. Ahn, A.J. Millis, Phys. Rev. B 58 (1998) 3697.
[40] K.I. Kugel, D.I. Khomskii, JETP Lett. 23 (1976) 237.
[41] S. Ishihara, M. Yamanaka, N. Nagaosa, Phys. Rev. B 55 (1997) 4206.